SYSTEMATIC NUMERICAL INVESTIGATIONS OF HEAT EXCHANGERS INTEGRATED BEHIND PROPELLERS OF HYBRID-ELECTRIC PROPULSION AIRCRAFT CONFIGURATIONS

J. Kirz*, A.-R. Hübner*, S. Spinner*
* German Aerospace Center (DLR), Institute of Aerodynamics and Flow Technology,
Lilienthalplatz 7, 38108 Braunschweig, Germany

Abstract

Hybrid-electric propulsion concepts have a great potential to reduce the overall emissions of aviation. For fuel cell applications heat exchangers are required to dissipate the waste heat produced by the fuel cell. The integration of heat exchangers has an impact on the aircraft aerodynamics which in turn is influencing the flow through the cooler duct. This paper applies a new method in the DLR TAU code to model a heat exchanger using the body force method in the Flowsimulator framework.
Integrating heat exchangers behind propellers generally has the benefit that heat can be dissipated even at low aircraft velocities due to the propeller slipstream. This paper analyzes integration effects of a cooler placed behind a propeller. The cooler position behind the propeller and the cooler duct shape are varied by adjusting the length and cross-sections of the diffuser, heat exchanger, and the nozzle.
The studies showed that the heat flux is mainly influenced by the outlet and inlet areas. The position of the components only has a minor impact on the heat flux but can be used to optimize the aerodynamic efficiency by avoiding flow separations and minimizing the drag. The results indicate that the slip stream can also have a negative effect on the cooler performance if the distance to the propeller is too low and local side slip angles get too high leading to flow separations.

Keywords

hybrid-electric; numerical simulation; propeller

NOMENCLATURE

Symbols

α	angle of attack	deg
c_f	skin friction coefficient	
D	Darcy coefficient	Pa · s / m^2
η	dynamic viscosity	Pa · s
$\vec{f}$	momentum source term	Pa/m
F	Forchheimer coefficient	kg / m^4
f_θ	energy source term	W
I	unit vector	
p	static pressure	Pa
$\dot{q}$	heat flux	W
ρ	density	kg/m^3
T	static air temperature	K
u, $\vec{u}$	velocity (vector)	m/s
U	velocity magnitude	m/s

Indices

∞	reference state
x	X direction
y	Y direction
z	Z direction

Abbreviations

BFHEX	Body Force Heat Exchanger Framework
CAD	Computer Aided Design
CFD	Computational Fluid Dynamics
HEP	Hybrid-Electric Propulsion
HEX	Heat Exchanger

1. INTRODUCTION AND OBJECTIVE

The European Green Deal targets a reduction of net greenhouse gas emissions by at least 55% by 2030 when compared to 1990 levels. Current studies suggest that aviation is responsible for about 3.3% of the

doi: 10.25967/610201

total CO_2 emissions [1]. In order to achieve the goals of the green deal and reduce CO_2 emissions for aircraft new propulsion concepts are proposed which include hydrogen and electric flight.
In 2020, DLR published the white paper 'Zero Emission Aviation' together with the German Aerospace Industries Association (BDLI) [2] and is currently working on a Zero Emission strategy. The European Commission launched a new Alliance for Zero Emission Aviation during 2020 as an initiative to prepare Europe for hydrogen and electric flight.
Some of the novel aircraft concepts utilize hybrid-electric propulsion (HEP) whereby electric motors are used to drive a propeller or fan and a fuel cell is installed to generate the electrical power for the motors. Studies show that aircraft powered by a hydrogen fuel cell have the potential to reduce the total climate impact by 75-90% when compared to kerosene-powered aircraft [3].
While the overall energy efficiency of hydrogen hybrid-electric aircraft is superior to conventional aircraft, current fuel cells achieve efficiency levels of about 40-60% depending on the fuel cell type [4]. Consequently, a significant share of the energy stored in the fuel is converted into waste heat. Thus, a heat exchanger integrated into a fairing cooler is required for heat dissipation. This presents an additional requirement for aircraft design and certification.
Three cooling concepts that are currently discussed are surface heat dissipation, RamAir coolers and heat exchangers integrated behind propellers. For these cooling concepts it becomes more and more important to numerically simulate and analyze heat exchanger designs integrated into complex aircraft geometries.
An important advantage of integrating the heat exchanger behind a propeller is that heat can be dissipated even at very low aircraft velocities due to the propeller slipstream. However, the simulation of the interactions between propeller and cooler is challenging. Established Computational Fluid Dynamics (CFD) codes must provide physically accurate and robust methods in order to assess the impact of the heat exchanger on the overall aircraft aerodynamics and vice versa.
Recently, DLR implemented a method to simulate heat exchangers in numerical simulations with the DLR TAU code based on a body force approach. The method was verified with analytical and OpenFOAM solutions [5] and already applied for an analysis of integration effects for a RamAir cooler concept [6].
This paper describes the challenges for the numerical simulation and aerodynamic integration of a cooler behind a propeller. Sensitivity studies with respect to the geometry of the cooler fairing are conducted.
In this paper the term *heat exchanger* will only refer to the actual heat exchanger while the term *cooler* will include the heat exchanger and the fairing consisting of the exterior, the lip, the diffuser, the nozzle and the trailing edge.

2. IMPLEMENTATION

Historically the DLR TAU code offered two methods to model a heat exchanger: The Heat Exchanger 1D boundary condition [7] and the Actuator Disk approach [8]. However, the methods are complicated to apply for the simulation of heat exchangers or were not robust for the challenging flow conditions of a heat exchanger integrated behind a propeller. Thus, in this work a method based on body force modeling using the Flowsimulator framework [9] is applied. It is based on a state of the art engine modeling method for the DLR TAU code [10] which has been modified and applied for the simulation of heat exchangers [5].
The Flowsimulator framework is coupled to the DLR TAU code via a Python interface. The body force modeling utilizes this interface to introduce volume specific source terms into the RANS equations and in TAU it has been mainly applied to simulate conventional turbofan engines. Previous studies have shown that carefully defined body force source terms are able to accurately model mean aerodynamic performance in turbo-machinery flow for different flow conditions operating points [10]. Therefore, it was suggested that the body forces approach would also be suitable for the modeling of heat exchangers. Due to its capability to resolve three-dimensional effects, it has the potential to be superior to 1D boundary conditions or actuator disk approaches. The approach taken is similar to that adopted in other CFD codes, such as CFX, as well as OpenFOAM.
The body force interface was extended according to the physics of a heat exchanger (HEX). The implementation is based on a filtering of the grid to identify the cells where HEX source terms are active. A source term $\vec{f}$ is added to the momentum equations while a source term f_θ for the heat flux is added to the energy equation within a filtered volume. More details about the source terms specified for the body force method are provided in Ref [11].
A heat exchanger is typically characterized by integral parameters like a pressure drop Δp and a heat flux $\dot{q}$. Three different ways to account for this pressure drop and heat flux are implemented:

1) **Fixed**
   Constant values of the integral pressure drop Δp and integral heat flux $\dot{q}$ are specified by the user.
2) **Lookup Table**
   The Flowsimulator Python framework is coupled to a lookup table derived from a 1D-model of the heat exchanger. Integral values for the pressure drop $\Delta p(p, T, U)$ and heat flux $\dot{q}(p, T, U)$ are calculated based on the average flow state one cell in front of the heat exchanger.
3) **Darcy-Forchheimer**
   The pressure drop Δp and heat flux $\dot{q}$ are calculated locally based on the Darcy-Forchheimer equation and a heat flux model.

For methods 1 and 2 a uniform distribution of the added momentum and energy within the filtered volume is assumed. Methods 2 and 3 both include an iterative approach to calculate the heat exchanger performance within the CFD simulation based on flow states through the cooler. In recent publications methods 1 and 3 were verified with analytical solutions as well as reference computations generated with OpenFOAM for a simple test case [5]. The focus of this paper is method 3, which is described in the following paragraphs.

Earlier versions of the body force heat exchanger (BFHEX) simplified the complex flow through the heat exchanger by specifying a fixed heat flux to the volume and adding a one-dimensional source term to the momentum equation. The pressure drop Δp for a heat exchanger with the length dx was calculated from the Darcy-Forchheimer equation by specifying the permeability coefficients K and k_2 [12]:

$$-\frac{dp}{dx} = \frac{\eta}{K} u_x + \frac{\rho}{k_2} u_x^2, \tag{1}$$

where η is the dyamic viscosity, ρ is the density, and u is the velocity. This one-dimensional approach works well as long as the velocity components normal to the heat exchanger primary axis are small. However, if the normal velocity components become significant or if separations occur, this method is no longer valid. As a consequence, in this paper a three-dimensional approach is applied by extending the Darcy-Forchheimer equation to three dimensions and calculating the momentum source term $\vec{f}$ for every cell:

$$\vec{f} = -\nabla p = [D + tr(\vec{u} \cdot I)\, F\,]\, \vec{u}. \tag{2}$$

By specifying high values for the Darcy coefficient D and Forchheimer coefficient F in y and z direction, the velocity components normal to the heat exchanger primary axis can be eliminated which is a better approximation for the physics of a heat exchanger especially for cases with flow separations in the cooler duct.

The heat flux for every cell is approximated based on the local temperature T, the local velocity magnitude U, the coolant inflow temperature $T_{Coolant}$, and the reference temperature T_∞ by the following equation:

$$f_\theta = \dot{q}_{max} \cdot \frac{U}{U + b} \cdot \frac{T_{Coolant} - T}{T_{Coolant} - T_\infty}, \tag{3}$$

where $\dot{q}_{max}$ is the asymptotic value for a theoretical maximum heat flux and b defines the slope of the function for velocities in the relevant range.

3. TEST CASE SETUP

A generic geometry with a propeller nacelle and a retro-fitted cooler is used as a test case. Initial studies with a cooler integrated into the nacelle of the engine showed a significant impact of flow separations in the cooler diffuser due to sensibilities to the curvature of the upper diffuser shape. Thus, in this work the cooler is modeled detached from the nacelle. Figure 1 shows the baseline test case geometry which is designed as a static CAD model for the propeller nacelle and a fully parametric CAD model for the cooler. The propeller is modeled using the actuator disk approach [8]. The heat exchanger is highlighted in orange.

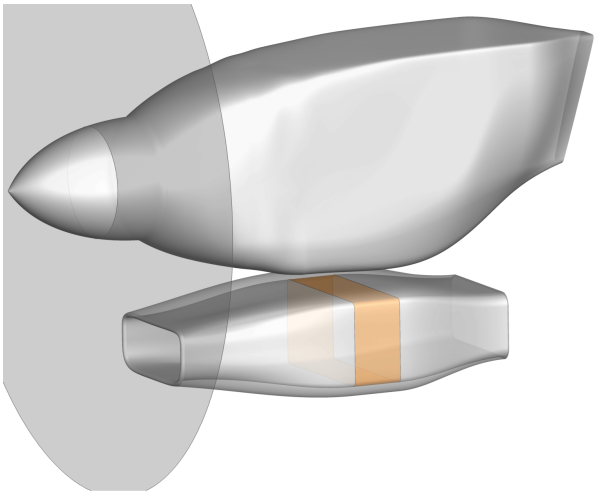

FIG 1. Generic nacelle and cooler test case geometry (orange: cooler).

The dimensions of the heat exchanger are approximately 0.2m x 0.6m x 0.3m (length x width x height) including 20mm rounded edges. The length of the cooler for the baseline case is 1.45m. The dimensions of the inlet are 0.5m x 0.2m (width x height) and the dimensions of the outlet are 0.5m x 0.25m (width x height) for the baseline case. The center points of the inlet, heat exchanger, and outlet are aligned on the same axis for the baseline case. The inlet is located 0.25m behind the actuator disk at a radial position of approximately 55%.

A clean geometry without the entire cooler is analyzed in addition to the baseline geometry and the parameter variations. Figure 2 shows a visualization of the parameters that were varied. While most cases are symmetric, two cases were analyzed where the inlet was inclined towards the propeller slip stream.

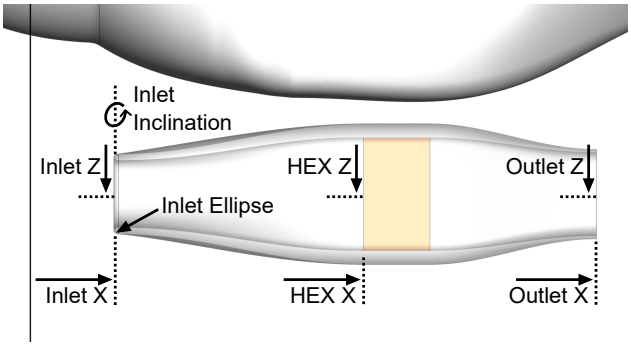

FIG 2. Overview of the parameterization.

3.1. Grid Generation

The commercial grid generation software CENTAUR was used to generate hybrid grids of the test case. The boundary layer is resolved with prisms while tetrahedra are used for the remaining volume. Sources are used to refine the tetrahedra behind the actuator disk to resolve the propeller slip stream, as shown in Figure 3.

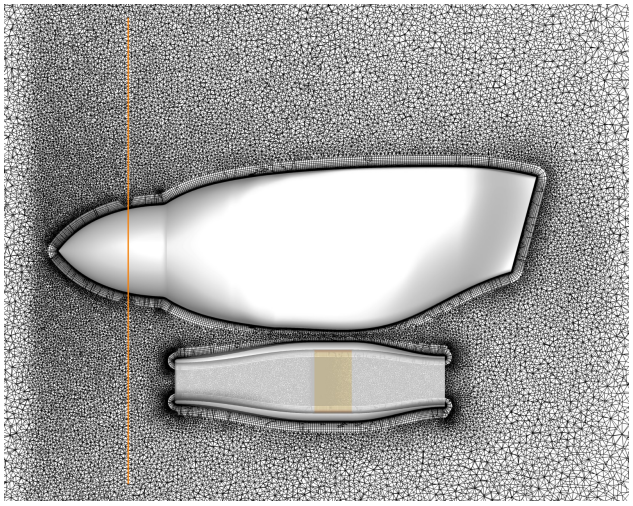

FIG 3. Overview of the grid (cut through symmetry plane).

Additionally, the volume within the cooler is refined and a very fine resolution is set at the inlet to the heat exchanger volume, as shown in Figure 4. The CATIA to CENTAUR sources tool [13] is applied to adjust the source positions for lip and heat exchanger refinement automatically when modifying the cooler geometry. The final grids have approximately 14.5 million nodes.

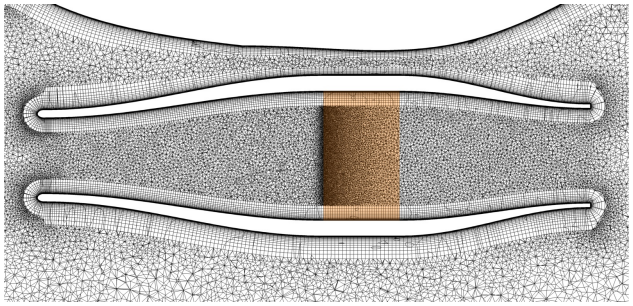

FIG 4. Grid in vicinity of the cooler with refined cells near the heat exchanger inlet.

3.2. Numerical Setup

The DLR TAU code [14] is a vertex-based CFD solver based on an unstructured finite-volume approach for solving the Euler or Reynolds-averaged Navier-Stokes (RANS) equations on hybrid grids. It was primarily developed for external aerodynamic applications. All TAU simulations presented in this paper were performed fully turbulent using the Spalart-Allmaras one-equation turbulence model [15] in negative formulation [16]. A second order central differencing scheme with matrix dissipation is applied for the spatial discretization of the convective fluxes and an implicit lower upper symmetric Gauss Seidel scheme is used for time stepping.
Initial studies analyzed the impact of different heat exchanger setups on the convergence behaviour of the simulation. Focus of these studies were the normal components of the Darcy and Forchheimer coefficients as well as the relaxation factors and coupling of the BFHEX method to the flow solver. Due to its linear contribution to the momentum equation the Darcy coefficient showed to be more effective to eliminate small normal velocity component fluctuations. However, if the normal components of the Darcy coefficient were increased too much, the convergence was less favorable.

Parameter	Value
Darcy coefficient D	[250, 1e5, 1e5]
Forchheimer coefficient F	[50, 0, 0]
Momentum relaxation factor	0.01
Coupling inner iterations	10
Number of coupling steps	5000

TAB 1. Overview of the heat exchanger setup.

A very tight coupling of the BFHEX method to the flow solver every 10 iterations together with a small relaxation factor for the momentum terms of 0.01 showed the best convergence behavior. A total number of 5000 coupling iterations was required to achieve a good convergence which is equivalent to 50,000 flow solver iterations. The final setup used for the simulations of the heat exchanger are summarized in Table 1. The heat flux coefficients are not specified here because they only have a minor influence on the aerodynamic performance and the heat flux can be directly scaled with $\dot{q}_{max}$ and the coolant temperature $T_{Coolant}$ (see equation 3). The resulting convergence plot for the heat exchanger is shown in Figure 5.

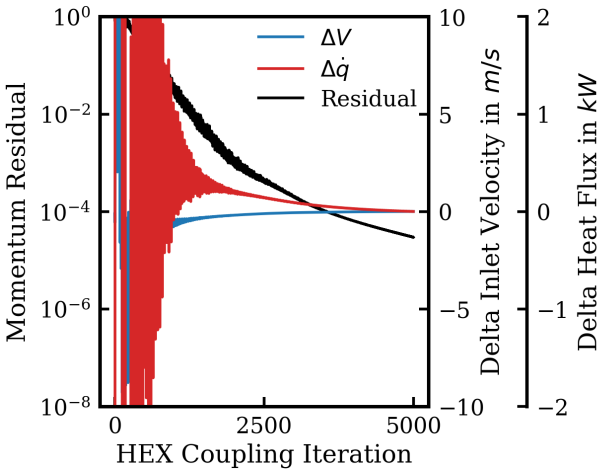

FIG 5. Convergence of the heat exchanger model.

4. INTEGRATION EFFECTS

Hybrid-electric propulsion concepts have a high demand for energy and therefore also cooling performance at take-off conditions. Since the velocity of the aircraft is still low, RamAir concepts often require large heat exchangers to fulfill the cooling requirement. Integrating the heat exchanger in the slip stream of a propeller has the advantage that a flow through the heat exchanger is maintained at take-off even at very low aircraft speeds as long as the propeller is generating thrust.
In order to get a better understanding of the integration effects, simulations have been performed with and without the cooler. Two main effects can be observed which will be essential to understand the parameter variation in the following section. As shown in Figure 6 and Figure 7 the flow between the nacelle and the cooler is accelerated due to the channeling effect. As a consequence, when the area behind the tightest cross section of the channel increases again, a pressure-induced flow separation occurs at the aft part of the nacelle which increases the drag of the nacelle.

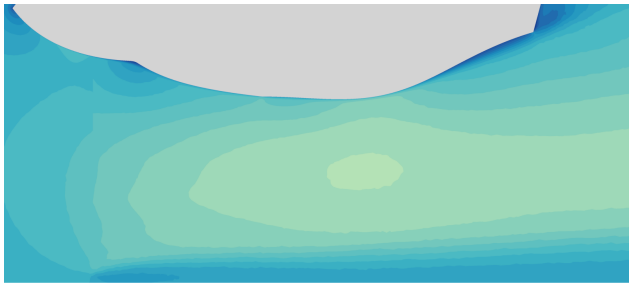

FIG 6. Mach number contours in the symmetry plane for the geometry without a cooler.

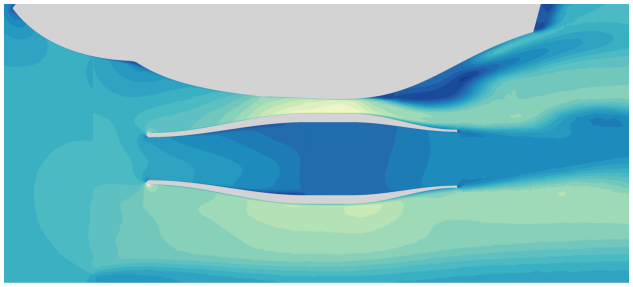

FIG 7. Mach number contours in the symmetry plane for the baseline cooler geometry.

The second effect can be observed in Figure 8, which shows areas with a negative skin friction coefficient in x direction and indicates areas of separated flow. A large flow separation occurs inside of the nacelle. The reason for this separation can be observed in Figure 9. Due to the propeller slip stream the flow approaches the cooler nacelle with a side slip angle of more than 12 degrees. The flow into the nacelle cannot follow this angle and separates from the side wall. However, the figure also demonstrates how the Darcy-Forchheimer equation with high coefficients normal to the main heat exchanger axis leads to a damping of the normal velocity components and a rectification of the flow within the heat exchanger.

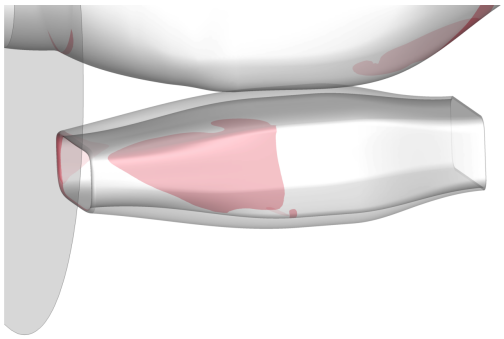

FIG 8. Areas with $c_{f,x} < 0$ indication for flow separations for the baseline case.

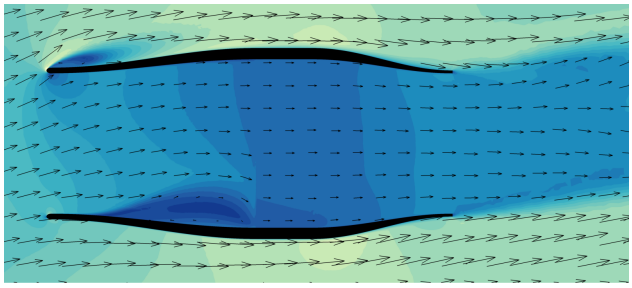

FIG 9. Velocity vectors in a horizontal plane through the middle of the heat exchanger of the baseline case.

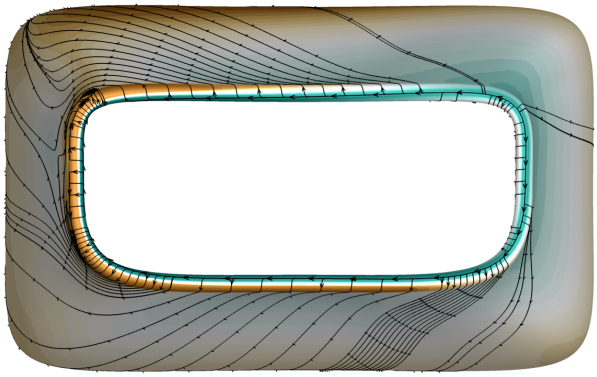

FIG 10. Pressure coefficient and stagnation line at the lip of the baseline geometry.

The position of the stagnation line on the inlet lip is shown in Figure 10. While the stagnation line is centered on the lip on the right side of the figure, it moves significantly inwards into the inlet geometry on the left side of the figure. As a consequence, the flow detaches on the exterior of the cooler on the left side which can also be observed as red area in Figure 8 and as detached flow in Figure 9.

Description	Varied Parameters	Values (difference to baseline)	Unit
Inlet X offset	Inlet X position	-50, 0, 50, 150, 250, 400, 500	mm
Inlet Z offset	Inlet Z position	-100, -50, 0, 50, 100	mm
HEX X offset	HEX X position	-200, -100, 0, 100, 200	mm
HEX Z offset	HEX Z position	-100, -50, 0, 50	mm
Outlet X offset	Outlet X position	-200, -100, 0, 100, 200	mm
Outlet Z offset	Outlet Z position	-100, -50, 0, 50, 100	mm
Inlet ellipse dX	Inlet ellipse dX	-5, 0, 5, 10, 15	mm
Inlet ellipse dZ	Inlet ellipse dZ	-10, -5, 0, 5, 10	mm
Inlet width	Inlet width	-40, -20, -10, 0, 10, 20, 40	%
Inlet height	Inlet height	-25, 0, 25, 50	%
Outlet width	Outlet width	-20, -10, 0, 10, 20	%
Outlet height	Outlet height	-40, -20, 0, 20, 40	%
Inlet inclination	Inlet inclination	0, 6, 12	deg
Short diffuser	HEX and outlet X position	-500, -400,-300, -200, -100, 0	mm
Diffuser curvature reduction	HEX and outlet Z position	-100, -50, 0	mm
X offset	Inlet, HEX, and outlet X position	0, 50, 150, 250, 400, 500	mm
Z offset	Inlet, HEX, and outlet X position	-300, -200, -150, -100, -50, 0	mm

TAB 2. Overview of the parameter variations.

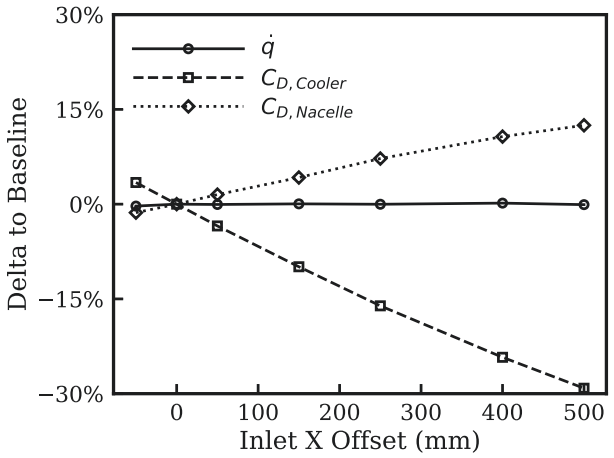

FIG 11. Inlet moved in x direction (short diffuser, position of HEX and outlet not changed).

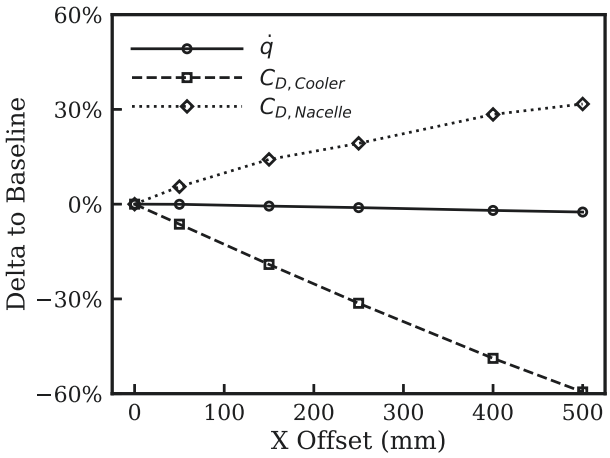

FIG 12. Complete cooler moved in x direction.

5. PARAMETER STUDY

The observed effects limit the performance of the cooler. In order to further assess and quantify the aerodynamic correlations of the heat exchanger integrated behind a propeller a large parameter study is conducted. Geometrical parameters of the cooler are varied and the impact on the heat flux and drag coefficients is analyzed. The values for the parameters are summarized in Table 2.

The drag coefficients shown in the following sections for the cooler components and resulting from the heat exchanger pressure drop will all be normalized by the drag coefficient of the baseline cooler including the heat exchanger pressure drop. Decreasing the drag of the cooler will often lead to increased drag of the propeller nacelle due to the tight coupling and interactions of these components. Thus, in the following sections the drag of the nacelle is always also considered when the cooler drag is discussed and plots show both, the cooler drag coefficient as well as the nacelle drag coefficient. The influence of the inlet ellipse parameters on heat flux and drag coefficient was minor and thus is not presented in this paper.

5.1. Horizontal Position Offsets

The baseline case includes only a small distance between the cooler lip and the actuator disk. In a first study the impact of varied x positions of the inlet, heat exchanger, and outlet is analyzed. Figure 11 shows the heat flux if the inlet is moved further away from the propeller.

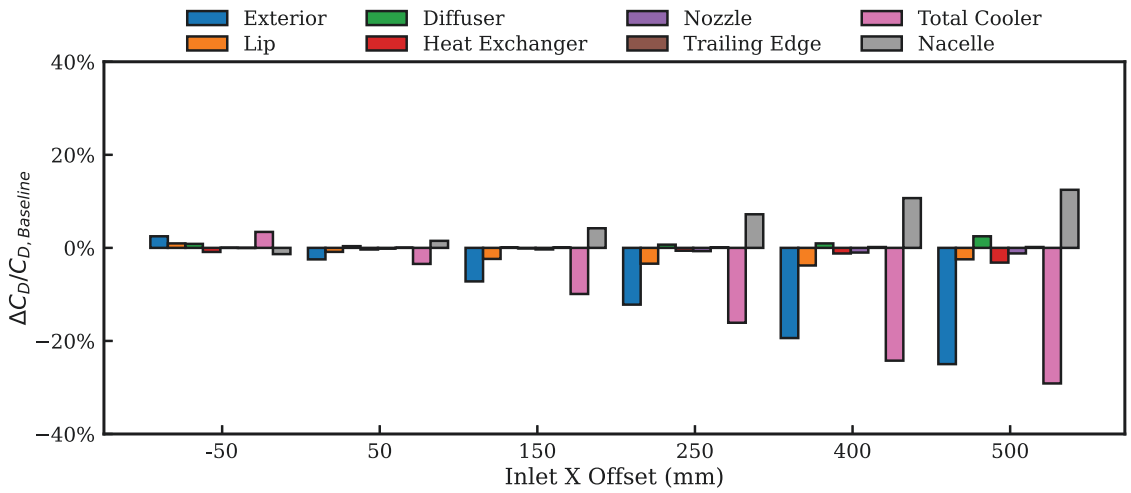

FIG 13. Impact of the different components on the total drag of the cooler compared to the nacelle drag for varied inlet x-positions.

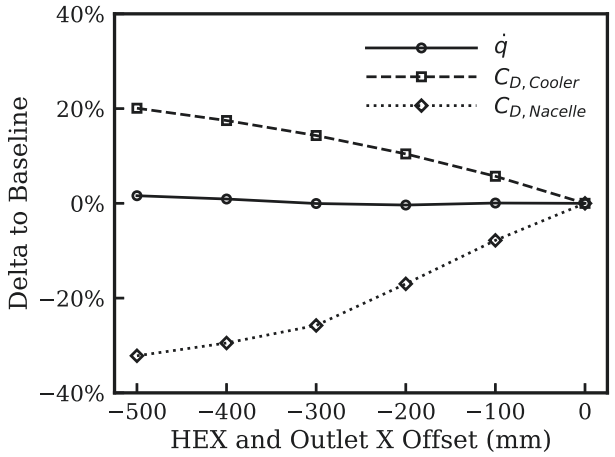

FIG 14. HEX and outlet moved in x direction (short diffuser, position of inlet not changed).

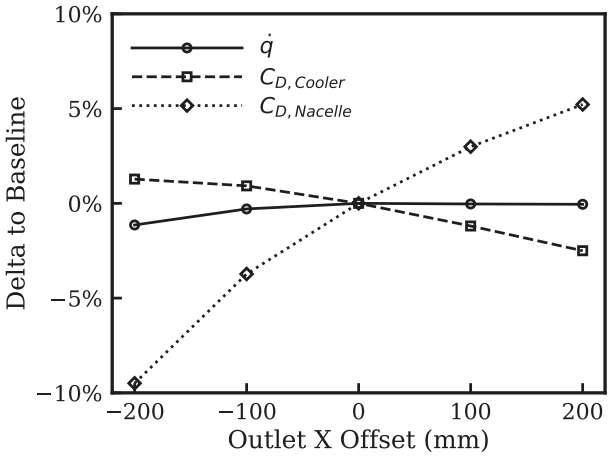

FIG 15. Outlet moved in x direction (position of inlet and HEX not changed).

Since the position of the heat exchanger and the outlet remain unchanged, the length of the diffuser is also reduced. The heat flux is not influenced by this position variation at all. However, the drag coefficients are significantly impacted. The drag of the cooler is reduced by up to 30% if the cooler is moved 500mm further away from the propeller disk. Although the drag of the nacelle is increased, the reduced drag at the cooler is approximately twice as high. Thus, a benefit of about 15% remains when moving the inlet further aft. The reason for this is that the acceleration of the flow in the duct between the cooler and the nacelle is beneficial for the drag of the cooler exterior if the inlet is moved further aft, as can be seen in Figure 13. A similar result can be achieved by moving the complete cooler away from the propeller, as shown in Figure 12. For the same distance the reduction of the drag is even higher when moving the whole heat exchanger further away from the propeller.

The same cooler geometry with a short diffuser duct that was discussed in Figure 11 can be obtained by moving the heat exchanger and the outlet towards the propeller while keeping the inlet position constant. The results of this variation are shown in Figure 14. The only geometrical difference to Figure 11 is the position of the geometry. However, in this case the impact of the nacelle drag is higher than the impact of the cooler drag. Again, a significant reduction in drag can be achieved by reducing the length of the diffuser.

Finally, the position of the outlet is varied, as shown in Figure 15. On the one hand the drag coefficient for the cooler increases if the length of the nozzle is decreased. On the other hand the drag of the nacelle decreases significantly. Thus, the total drag can be reduced by up to 10% when reducing the length of the nozzle by 200mm with only a minor impact on heat flux. The impact of the x-position of the HEX is not shown here but shows a similar trend as the outlet x-position.

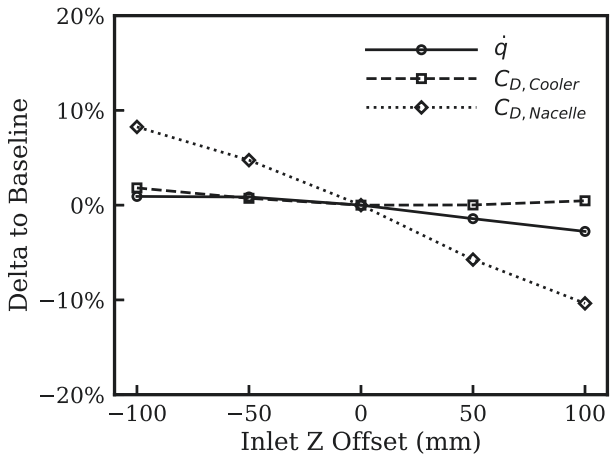

FIG 16. HEX performance for Inlet moved in z direction (HEX and outlet not changed).

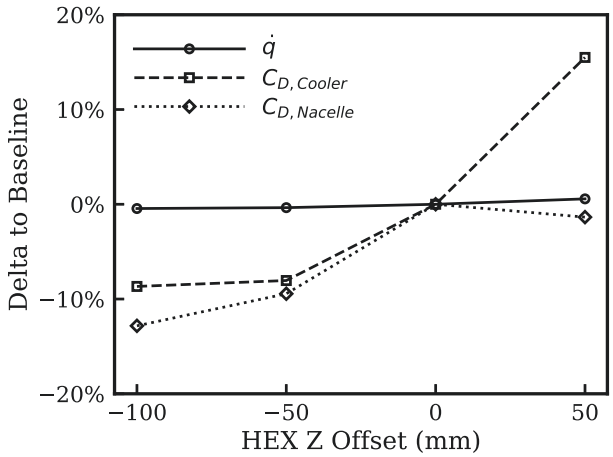

FIG 17. HEX performance for HEX moved in z direction (inlet and outlet not changed).

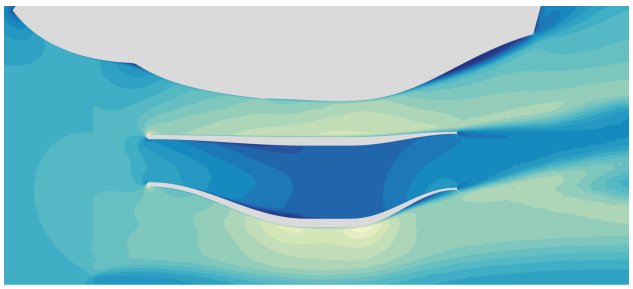

FIG 18. Mach number contours in the symmetry plane if the HEX is lowered by 100mm.

5.2. Vertical Position Offsets

The z-positions of the cooler components influence both, the curvature in the duct as well as the flow around the cooler and interactions with the engine nacelle. Figure 16 shows that the impact of the z-position variation of the inlet on the drag coefficient of the cooler is minor. The inlet z-position mainly influences the drag of the nacelle. In contrast to this, lowering the mid part of the cooler including the heat exchanger has a significant potential to reduce the drag.

Figure 17 shows a drag reduction of 8% for the cooler and 12% for the nacelle if the heat exchanger is lowered to the lowest analyzed position. This can be explained by the channel between the engine nacelle and the cooler that is widened up when lowering the mid part of the cooler resulting in less interference. The symmetry plane Mach number contours in Figure 18 visualize this effect. Furthermore, the analysis of the individual drag components showed that not only the exterior drag was decreased but also the drag of the diffuser.

In contrast to this, when only adjusting the vertical position of the outlet (see Figure 19) the drag decreases if the outlet is placed further up. In this case, the minimal channel area between the engine nacelle and cooler is given by the position of the heat exchanger. Only the magnitude of the following expansion is controlled by the outer shape of the nozzle with the potential to eliminate the flow separation at the engine nacelle. As a consequence, the drag of the cooler can be decreased by 10% and the drag of the nacelle can be reduced by 5% if the center of the outlet is placed 100mm above the center of the heat exchanger.

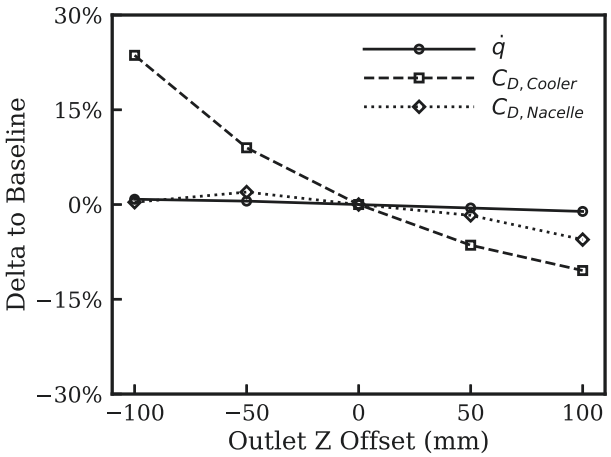

FIG 19. HEX performance for Outlet moved in z direction (inlet and HEX not changed).

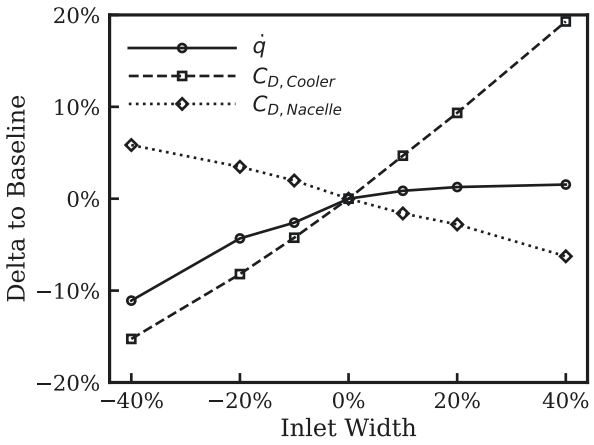

FIG 20. HEX performance for varied inlet widths.

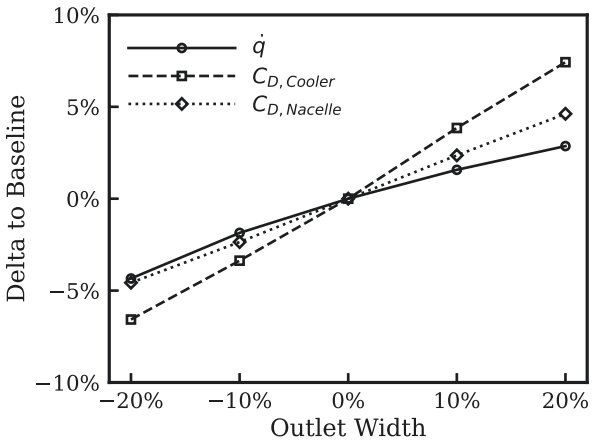

FIG 22. HEX performance for varied outlet widths.

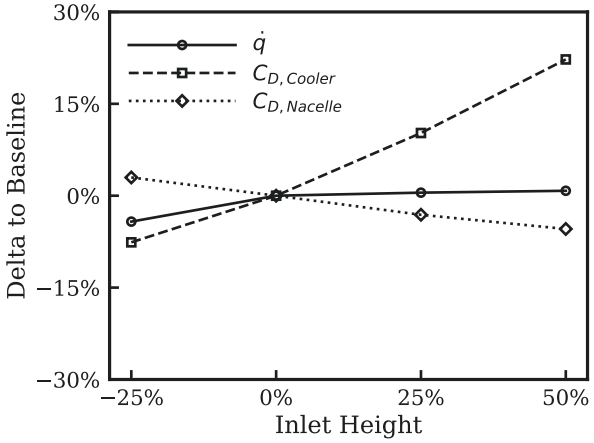

FIG 21. HEX performance for varied inlet heights.

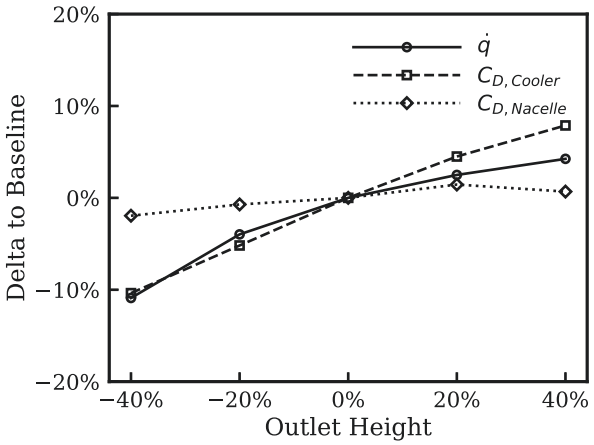

FIG 23. HEX performance for varied inlet heights.

5.3. Impact of the Inlet and Outlet Area

Previous studies for a fuselage mounted cooler without the implementation of the Darcy-Forchheimer equation showed how important an appropriate inlet and outlet area is for the achievable mass flow rate and the performance of the heat exchanger [6]. In order to verify these studies, the height and width of the inlet and outlet were varied.

Figure 20 shows the influence of the inlet width on the cooler performance while Figure 21 shows the impact of the inlet height. A linear correlation between the inlet width or the inlet height and the drag can be observed. The heat flux shows an asymptotic trend with increasing inlet area, indicating that an optimum area exists for a specific heat flux requirement. The integration drag on the engine nacelle decreases with increased inlet area. The outlet behaves slightly different, as shown in Figure 22 and Figure 23. Generally, increasing the outlet area results in a higher mass flow rate and consequently a higher heat flux. However, reducing the outlet area is very efficient compared to the inlet area because the drag of the cooler decreases in the same direction as the nacelle drag. Reducing the outlet width results in the highest benefit.

The wide inlet is the only case out of all parameter variations where the area of separated flow inside the cooler duct is small, as shown in Figures 25 and 26. However, the overall efficiency of this case is not very good because the heat flux does not further increase while leading to a significant drag penalty from the diffuser, as shown in Figure 24. Thus, from a design perspective it might not be possible to ensure attached flow within the whole cooler duct for a good performance behind a propeller with shaping techniques presented in this paper. However, more complex techniques like guiding vanes or an advanced internal cooler design might be able to achieve attached flow in the diffuser duct even with smaller inlet areas which is out of scope of this activity.

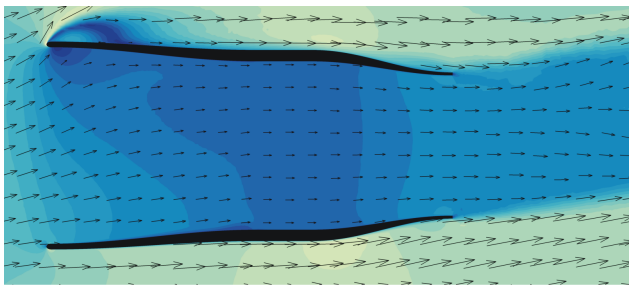

FIG 25. Velocity vectors in a horizontal plane through the middle of the heat exchanger of the case with a very wide inlet (+40% inlet area).

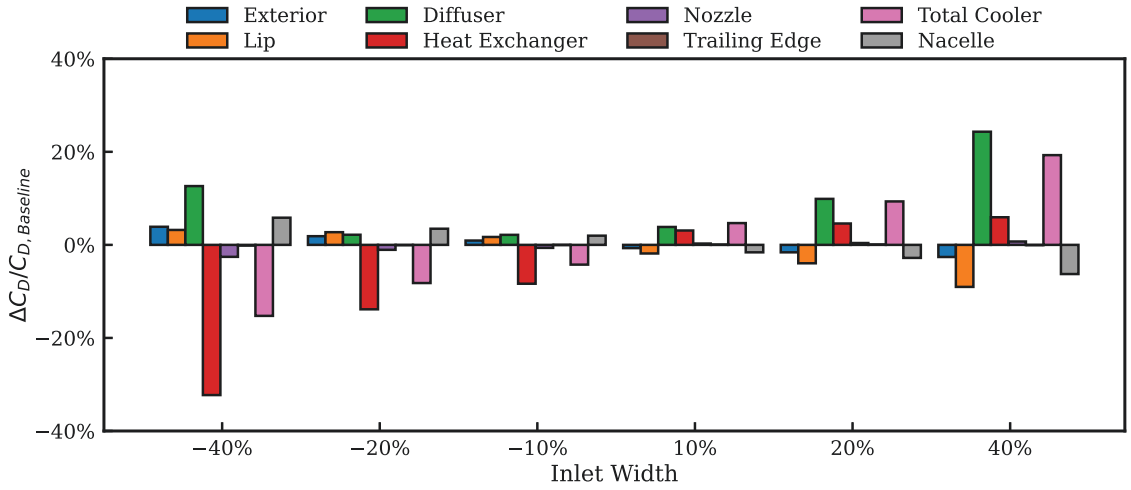

FIG 24. Impact of the different components on the total drag of the cooler compared to the nacelle drag for varied inlet widths.

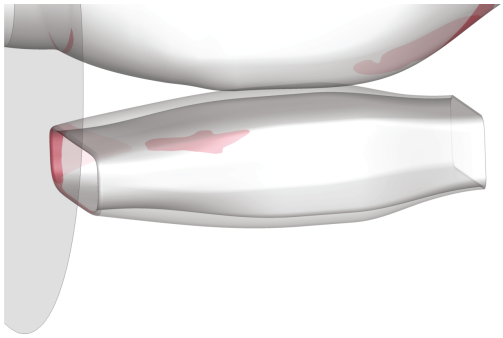

FIG 26. Areas with $c_{f,x} < 0$ indication for flow separations for the case with a very wide inlet (+40% inlet area).

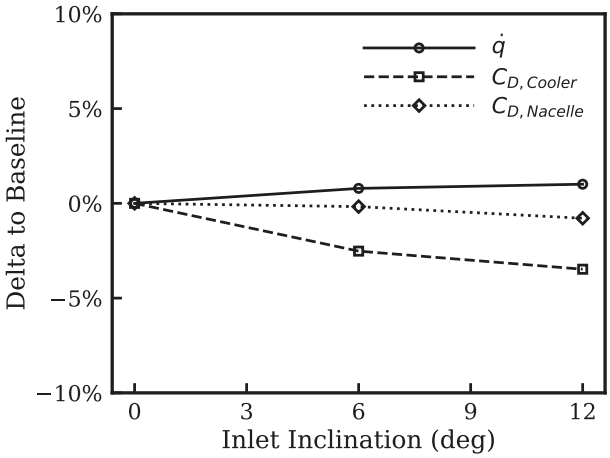

FIG 27. Inlet inclination angle.

5.4. Impact of the Inlet Inclination Angle

The inclination angle has a great potential to account for the slip stream of the propeller. Two simulations were performed with 6° and 12° inclination. Figure 27 shows the impact of this modification on the heat exchanger performance. The 12° inclination case slightly increases the heat flux while reducing the drag of both, the cooler and the nacelle. This can be explained by the reduction of exterior drag of the cooler because the flow separation on the leeward side of the cooler is not occurring in this case, as shown in Figure 28 and 29. However, the flow separation in the diffuser could not be resolved.

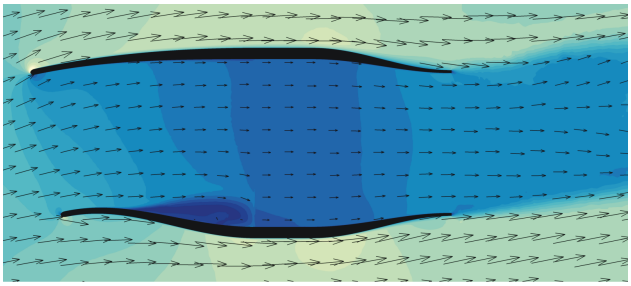

FIG 28. Velocity vectors in a horizontal plane through the middle of the heat exchanger of the case with an inclined inlet (12°).

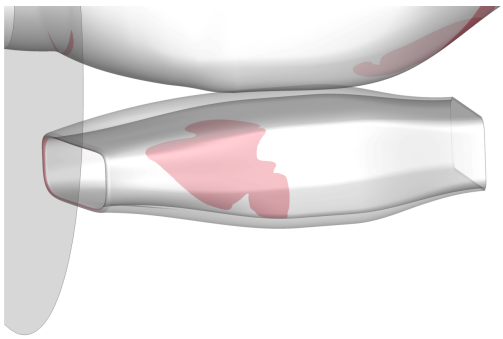

FIG 29. Areas with $c_{f,x} < 0$ indication for flow separations for the case with an inclined inlet (12°).

6. SUMMARY AND OUTLOOK

In this paper, a new implementation of the Darcy-Forchheimer equation as source term for the body force model in the Flowsimulator framework of the DLR TAU code has been presented. Integration effects of a cooler installed below the engine nacelle of a hybrid-electric aircraft concept have been studied. The detached integration of the cooler for the selected engine nacelle geometry showed negative integration effects in the form of flow separation in the aft part of the engine nacelle.
The main challenge for the integration of the cooler behind the propeller remains to control the flow separations at the cooler due to the propeller slip stream. Their impact could only be decreased with a very large inlet area which resulted in a significant drag penalty. Although the separations could not be fully avoided, cases were identified where the drag was significantly reduced. The possibilities include placing the heat exchanger at a larger distance behind the propeller or placing the heat exchanger slightly lower in the duct to avoid pressure induced flow separations due to the curvature at critical points.
In conclusion, the studies showed that the heat flux is mainly defined by the outlet and inlet areas. The position of the components only has a minor impact on the heat flux but can be used to optimize the drag. For the design of heat exchangers integrated into cooler fairings behind the engine this shows that the most important step is to determine efficient areas for the inlet and outlet based on a heat exchanger geometry and the heat flux requirements.
The next steps will be to run an optimization of the cooler geometry and improve the nacelle geometry. Once the aerodynamic effects of the detached cooler are fully understood the heat exchanger will be integrated into the engine nacelle.

7. ACKNOWLEDGEMENTS

This work has received funding by the German Ministry of Economic Affairs and Climate Action (BMWK) on decision of the German Parliament in the frame of the HEPS project (funding reference no. 20M1912C).

The authors would like to thank Thomas Wernsdorfer and Keith Weinman for the very valuable support for the implementation and modeling of the heat exchanger. Furthermore, the authors do gratefully acknowledge the valuable discussions with MTU about the numerical simulation of heat exchangers.

Contact address:

jochen.kirz@dlr.de

References

[1] D. S. Lee, D. W. Fahey, M. R. Skowron, M. R. Allen, and U. Burkhardt. The contribution of global aviation to anthropogenic climate forcing for 2000 to 2018. *Atmospheric Environment*, 244:117834, 2021. DOI: 10.1016/j.atmosenv.2020.117834.

[2] DLR, BDLI. Zero emission aviation - german aviation research white paper. Technical report, 2020.

[3] McKinsey & Company. Hydrogen-powered aviation - a fact-based study of hydrogen technology. Technical report, 2020.

[4] EG&G Technical Services, Inc and U.S. Department of Energy. Fuel cell handbook. Technical report, 2004.

[5] Jochen Kirz, Andreas Huebner, Sebastian Spinner, and Keith Weinman. Application of a body force approach for numerical heat exchanger simulations within a hybrid electric propulsion aircraft concept. *CEAS Aeronautical Journal*, in review.

[6] Andreas Huebner and Jochen Kirz. Numerical prediction of heat exchanger performances for a hybrid electric propulsion aircraft concept. In *AIAA AVIATION 2023 Forum*, 2023. DOI: 10.2514/6.2023-3385.

[7] Bernhard Eisfeld and Markus Ruetten. A coupled heat exchanger boundary condition for predesign of air-intake positions. In *50th AIAA Aerospace Sciences Meeting*, Nashville, TN, 2012. DOI: 10.2514/6.2012-463.

[8] Axel Raichle, Stefan Melber-Wilkending, and Jan Himisch. A new actuator disk model for the tau code and application to a sailplane with a folding engine. In *STAB-Symposium*, 2006. DOI: 10.1007/978-3-540-74460-3_7.

[9] Michael Meinel and Gunnar Einarsson. The flowsimulator framework for massively parallel cfd applications. In *PARA 2010*, 06 2010.

[10] Sebastian Spinner, Marco Trost, and Rainer Schnell. An overview of high fidelity cfd engine modeling. In *AIAA SciTech*, San Diego, 2022. DOI: 10.2514/6.2022-0430.

[11] William Thollet. *Body Force Modeling of Fan-Airframe Interactions*. PhD thesis, Institut Supérieur de l'Aéronautique et de l'Espace Toulouse, 2017.

[12] Donald A. Nield and Adrian Bejan. *Convection in Porous Media*. Springer, 2013. DOI: 10.1007/978-1-4614-5541-7.

[13] Jochen Kirz. Surrogate based shape optimization of a low boom fuselage wing configuration. In *AIAA Paper 2019–3489*, 2019. DOI: 10.2514/6.2019-3489.

[14] Dieter Schwamborn, Thomas Gerhold, and Ralf Heinrich. The dlr tau-code: Recent applications in research and industry. In *ECCOMAS CFD 2006 CONFERENCE*, Delft, 2006.

[15] P. R. Spalart and S. R. Allmaras. A one-equation turbulence model for aerodynamic flows. In *30th Aerospace Sciences Meeting and Exhibit*, Reno, NV, 1992. DOI: 10.2514/6.1992-439.

[16] Steven Allmaras, Forrester Johnson, and Philippe Spalart. Modifications and clarifications for the implementation of the spalart-allmaras turbulence model. In *Seventh International Conference on Computational Fluid Dynamics (ICCFD7)*, pages 1–11, 01 2012.